MATERIALE PLASTICE
https://revmaterialeplastice.ro
https://doi.org/10.37358/Mat.Plast.1964

A Multifunctional Composites Membrane Aiming at Flexible Sensor and Ultrabroadband Electromagnetic Wave Absorption

GUANFA XIAO[1], ZHIHENG YU[2*], ZIMAO YAO[3]
[1] Ganzhou Lanxuan Technology Co., Ltd, Ganzhou 341000, China
[2] College of Mechanical and Electrical Engineering, Jiaxing Nanhu University, Jiaxing Zhejiang 314000, China
[3] School of Automotive Studies, Jiangxi College of Applied Technology, Ganzhou Jiangxi 341000, China

Abstract: *A study was conducted on SEBS-based composites granules containing different volume fractions of carbon nanotubes (CNTs) using a twin extruder and hot pressing procedure to produce a SEBS/CNTs membrane. SEM was used to study the membrane's morphology, revealing a 3-D network of CNTs. TGA was utilized to measure the degradation temperature of SEBS polymer and determine the actual volume fraction of CNTs. The mechanical properties, electrical conductivity, and cyclic strain sensing behavior of the SEBS/CNTs were investigated using a tensile testing machine and pico-ammeter. Mathematical models were used to fit the measured data, demonstrating the strain sensing potential of the composites. The composite membrane with 2 wt.% of CNTs exhibited superior electromagnetic wave absorption performance with a minimum reflection loss (RLmin) value. This study provides promising opportunities for the development of advanced materials.*

Keywords*: SEBS (styrene-ethylene-butylene-styrene), CNTs, Composites Membrane, Flexible Sensor, Electromagnetic Wave Absorption*

1. Introduction

SEBS (styrene-ethylene-butylene-styrene) block copolymer is a widely used thermoplastic elastomer due to its excellent mechanical properties, such as high elasticity, flexibility, and toughness [1-4]. In recent years, research on SEBS-based composites has focused on improving their properties, including electrical conductivity, thermal stability, and mechanical strength [5-8].

Carbon nanotubes (CNTs) have attracted significant attention as a promising material in various fields due to their unique mechanical, electrical, and thermal properties [9-11]. Therefore, researchers worldwide have extensively used SEBs resin to prepare various functional composite materials in combination with CNTs, thus developing strain sensors [12-16]. Besides, CNTs have been extensively studied in the field of electromagnetic wave (EMW) absorption due to their excellent EMW absorption performance [17-21]. Many studies have reported on the preparation and EMW absorption properties of CNT-based composites, which have shown promising results. However, the percolation threshold of CNTs in composites and the effect of CNT content on the mechanical and electrical properties of the composite materials have not been fully elucidated. Moreover, most of these studies have focused on either the strain sensoring behavior or the EMW absorption performance, and the comprehensive of the effect of SEBS/CNTs membrane composites has not been well investigated.

Therefore, in this study, we prepared SEBS/CNTs composite membranes with different CNT contents, including multi-wall CNTs, and investigated their mechanical, electrical, and EMW absorption properties. The results provide fundamental insights into the properties of SEBS/CNTs composites and demonstrate their potential for various applications, including EMW absorption and strain sensing.

2. Materials and methods

2.1. Preparation of SEBS/CNTs Composite Membranes

Kraton G-1780 was the SEBS polymer granules used in this study, while Orion Engineered Carbons Co., Ltd provided the carbon nanotubes. Both materials were dried at 80ºC for 96 h in a vacuum oven to eliminate any residual moisture. The raw materials were fed simultaneously into a co-rotating twin screw

**email: yuzhiheng@jxnhu.edu.cn*

extruder (Leistritz Micro-18/GL-40D) at 60 rpm and 120ºC, using a die with a diameter of 1 mm, until complete extrusion was achieved. The resulting composite filament was pelletized to produce the final composite granules. The SEBS/CNTs granules were stored in a vacuum atmosphere until further use. A Lauffer RMV-250 hot presser was used to produce the SEBS/CNTs granules into composite membranes under vacuum at the desired thickness. The membranes were cut into specimens measuring 40 mm x 1 mm for subsequent measurements. Figure 1 illustrates the process of producing the SEBS/CNTs membrane.

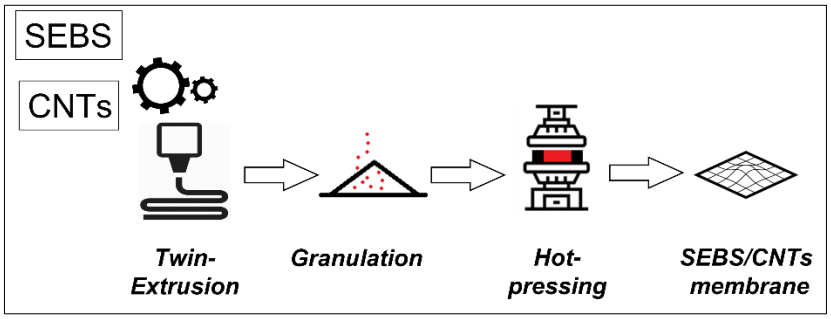

Figure 1. Experimental preparation flowchart in this study

2.2. Characterization

The morphologies of the SEBS/CNTs composite membrane were analyzed using a scanning electron microscope (ZEISS EVO). Prior to analysis, the specimens were coated with a thin layer of gold and then observed with a secondary electron detector at an acceleration voltage of 10 kV. The thermal stability of the specimens was evaluated using Thermogravimetric Analysis (TGA) (TA Instruments, 2960) under nitrogen atmosphere, from room temperature to 1000ºC at a heating rate of 10 ºC/min. The electromechanical properties of the samples were measured using a tensile testing machine (Zwick, Z005) coupled with a Keithley 6485 Picoammeter. As shown in Figure 2, the specimens were secured to the tensile testing machine with a gauge length of 20 mm, and the clapper was enclosed with several layers of isolated tape. A strain rate of 60 mm/min was applied during the dynamic resistance measurement while the specimens were stretched. At least 10 specimens were tested for the dynamic electromechanical measurement, and the data of at least 5 specimens were recorded for the cyclic strain sensing test. The electromagnetic parameters of the samples were evaluated using a vector network analyzer (Agilent N5234A, Keysight Technologies, Inc., USA). In this study, the following nomenclature was used to describe all the samples: CNT1.5 indicates the designed volume fraction of CNT in the composite was 1.5 vol. %, while Virgin represents the neat SEBS polymer that was extruded using the twin extruder under the same conditions as a contrast.

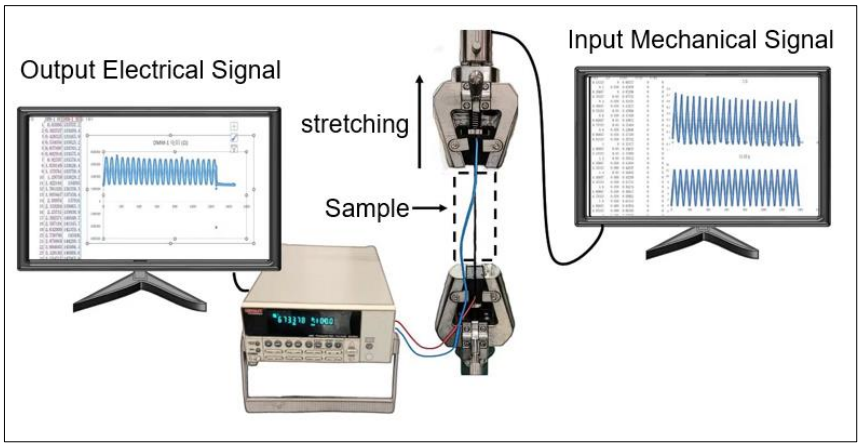

Figure 2. Schematic diagram of the tensile test setup used for measuring the input mechanical signal and the output electrical signal during stretching

3. Results and discussions

3.1. Morphologies

SEM analysis (Figure 3) was conducted to investigate the cross-sectional microstructures of the stretched SEBS/CNTs composite membrane. The hot-pressing technique used in the study resulted in most of the CNTs being covered by the polymer. A slight phase separation was observed between the SEBS/CNTs composite membrane regions that did not participate in the stretching process. Additionally, the zoomed-in image of the damaged region of the SEBS/CNTs composite membrane showed a well-dispersed CNTs in the SEBS matrix, indicating the effectiveness of the melt mixing procedure using the twin extruder.

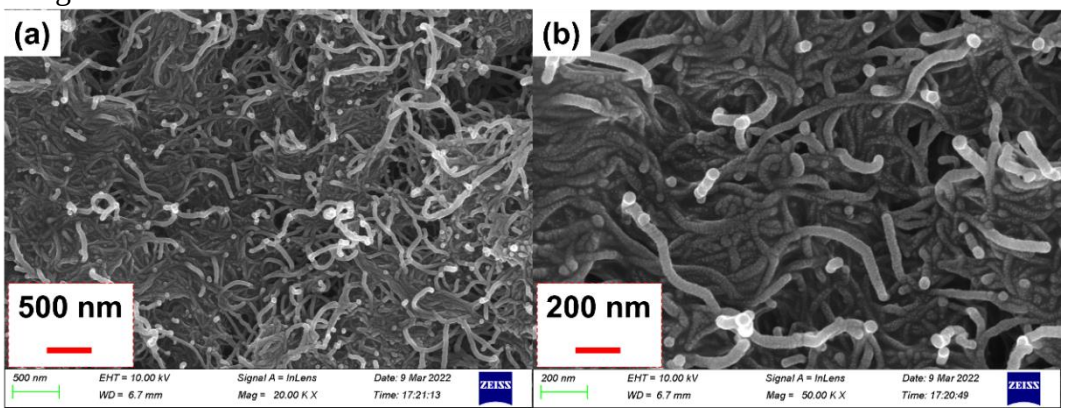

Figure 3. Cross-sectional SEM Images of the SEBS/CNTs Composite Membrane

3.2. Thermal Gravity Analysis of the SEBS/CNTs composite membrane

The TGA measurements of SEBS/CNTs composite membrane are presented in Figure 4, displaying the remained mass of all specimens against temperature in different colors. Notably, the weight reduction for all samples begins at around 400°C, which corresponds to the degradation temperature of SEBS and implies a practical temperature range for composite applications. Additionally, the weight percentage of the sample remains stable after 500°C, indicating the composition remaining in the sample after heat treatment. The value inserted in the figure represents the final remained weight of the samples, and the difference between this and the remained mass of the Virgin (approximately 0%) reflects the actual weight fraction of the CNTs in the composite.

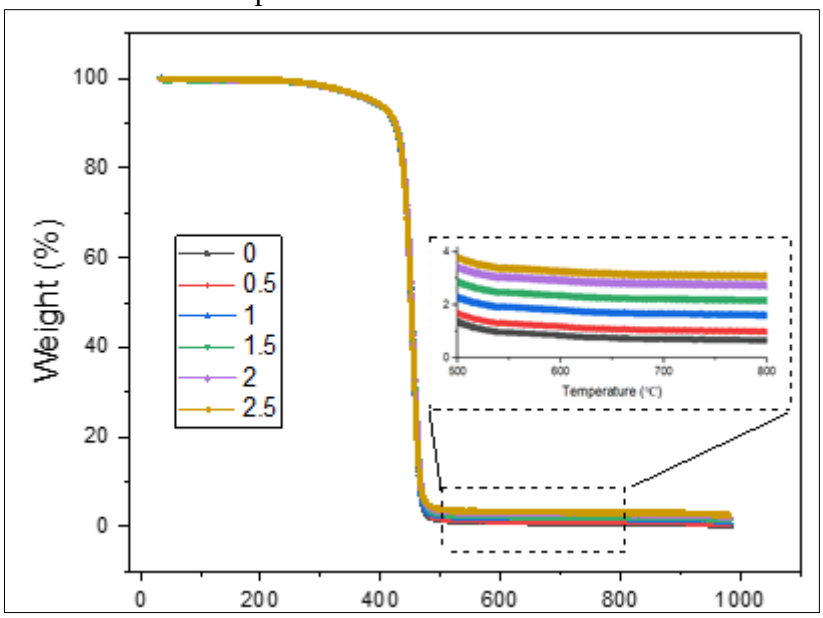

Figure 4. TGA measurement of SEBS/CNTs composite membranes for determining weight fraction and thermal behavior

3.3. Mechanical properties

Figure 5 displays the stress-strain curves obtained from the tensile testing machine for all six SEBS/CNTs composite membrane specimens. Notably, despite its flexibility, the SEBS/CNTs composite membrane exhibits a great strain range. The addition of CNTs results in decreased elongation at break compared to that of the virgin SEBS, and the membrane with 2.5% CNTs exhibits minimal elongation at break compared to the others. This is attributed to the hindrance of CNT particles in the construction of the continuous phase of the polymeric matrix, leading to lower elongation at break.

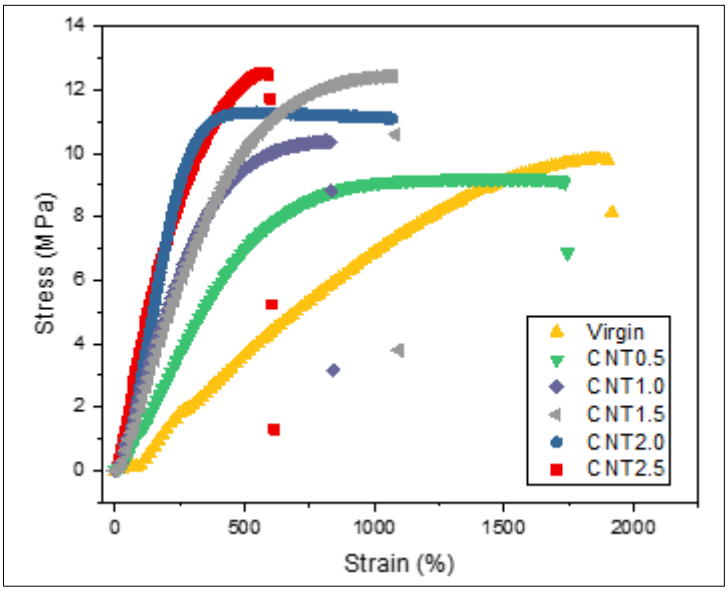

Figure 5. Stress-strain Curve of SEBS/CNTs composite membrane in this tudy

The Young's modulus of the samples was determined by calculating the slope of the first 20 points on the stress-strain curve of each sample, and the results are shown in Figure 6 in red. It is observed that with the increase in CNT content, the Young's modulus of the samples is significantly enhanced, as the higher fraction of CNTs in the samples contribute to the linear elastic deformation region of the samples.

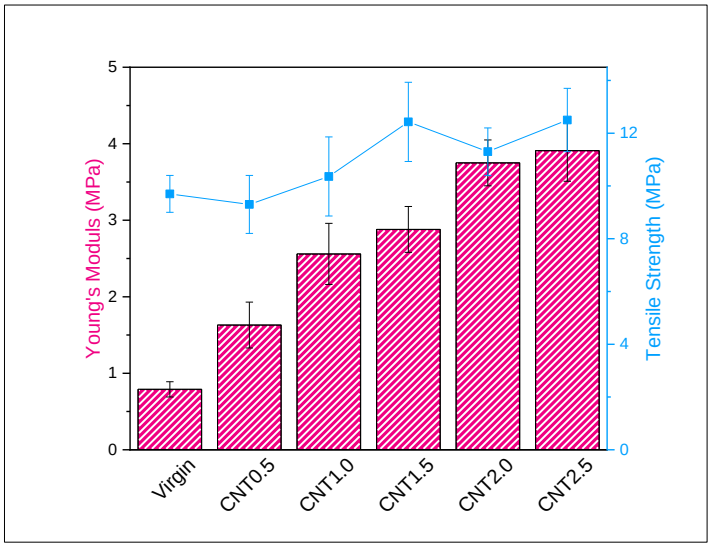

Figure 6. Young's modulus and tensile strength of SEBS/CNTs composites at varying CNTs fraction

3.4. Electrical Conductivity and Cyclic Strain Sensing Behavior of the SEBS/CNTs Composites Membrane

The electrical conductivity of SEBS composites increases with increasing CNT filler content. The percolation threshold, which represents the critical volume fraction of conductive fillers where the conductivity of the composite increases most rapidly, is used to describe this phenomenon. McLachlan's equation is a commonly used formula for calculating the percolation threshold in conductive composites [22, 23].

$$(1-\phi)\frac{{\sigma_m}^{1/s}-{\sigma_c}^{1/s}}{{\sigma_m}^{1/s}+{\sigma_c}^{1/s}(1-\phi_c)/\phi_c}+\phi\frac{{\sigma_f}^{1/t}-{\sigma_c}^{1/t}}{{\sigma_f}^{1/t}+\frac{1-\phi_c}{\phi_c}{\sigma_c}^{1/t}}=0 \quad (1)$$

$\sigma_m, \sigma_c, \sigma_f$ represent the conductivity of the SEBS matrix, SEBS/CNTs composite, and CNTs, respectively. ϕ is the volume fraction of CNTs, and ϕ_c is the critical volume concentration, i.e., the percolation threshold. The exponent t has a standard value of 0.87. For isotropic composites with randomly oriented fillers, the exponent s has a standard value of 2. However, in this study, s was set to 1.5 because the CNTs' distribution was not isotropic from a 3D perspective. Using equation 1, the value of ϕ_c was calculated as 1.73%.

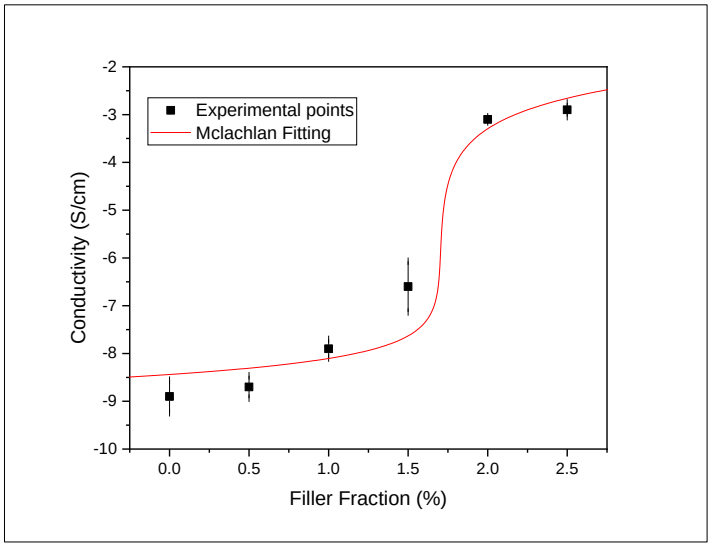

Figure 7. Volume fraction dependence of electrical conductivity for SEBS/CNTs composite membrane, fitted with McLachlan equation

In order to further study the electrical properties of the composites, specimens CNT2.0 and CNT2.5, which contain CNTs beyond the percolation threshold, were selected for cyclic sensoring experiments. The relative change in resistance (RCR) of the electrically conductive composites was calculated using the following formula [24-26]:

$$RCR=\frac{\Delta R}{R_0}=\frac{R-R_0}{R_0} \quad (2)$$

where the ΔR, R_0, and R denotes the change of the resistance, the initial resistance, and the resistance under strain in time, respectively.

Figure 8 displays the RCR values of specimen CNT2.5 and CNT2.0 under a strain of 50% during cyclic tests, shown in blue and red, respectively. The graph shows ten cycles, with clear periodicity observed for both specimens (10 output peaks). To facilitate comparison between the input strain signal and the output electrical signal, two dashed lines were included. The CNT2.5 specimen exhibited only

a slight delay between the input and output signals derived from the SEBS composites, indicating excellent repeatability and superior recoverability of the SEBS-based composites.

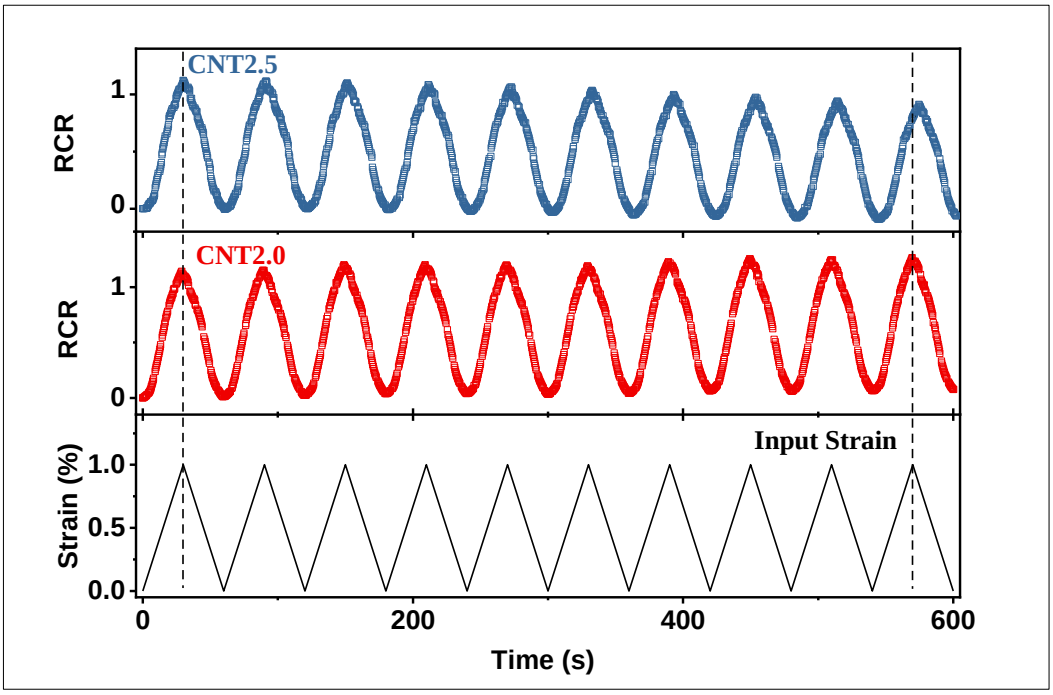

Fig.8 Graph of RCR value over time for CNT2.5 (blue) and CNT2.0 (red), recorded during 10 stretching cycles

Figure 9 provides a possible explanation for the observed delay in the output electrical signal of the CNT2.5 specimen. The diagram shows that during cyclic testing, the CNTs in the composite are subjected to mechanical deformation, resulting in a change in the distance between them [27]. As the strain increases, the distance between CNTs decreases, and the electrical conductivity of the composite increases accordingly. However, as the strain decreases, the distance between CNTs increases, resulting in a decrease in conductivity. This process takes time, which explains the delay observed in the electrical signal of the CNT2.5 specimen.

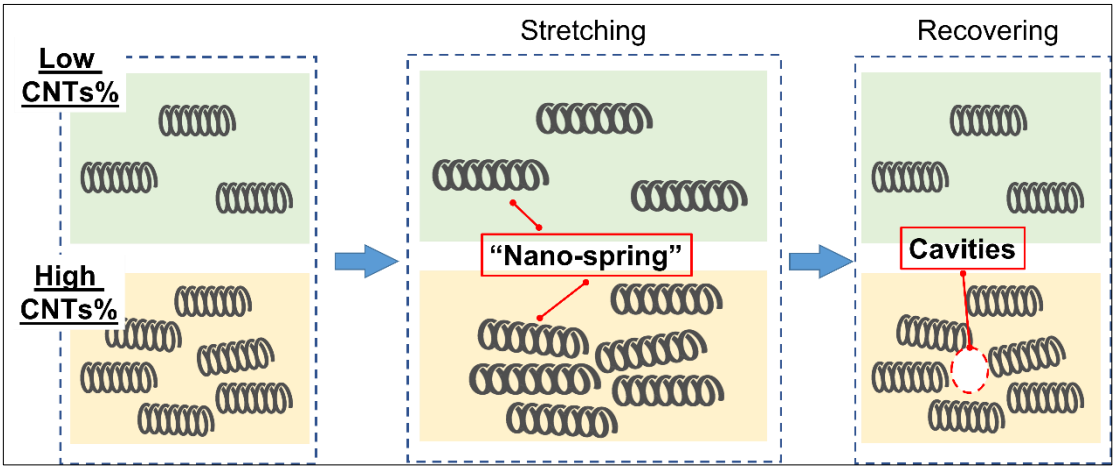

Figure 9. Diagram illustrating the change of the created cavity SEBS/CNTs composites during stretching

In order to further understand the delayed phenomenon observed in the RCR diagram of the CNT2.5 composite, a diagrammatic sketch was presented in Figure 9. The stretch and recovery processes of the

SEBS matrix were explained as a uniform elongation and recovery along the stretching direction, respectively. Meanwhile, the CNTs in the composite were considered as "nano-springs" that were also stretched along the same direction during the stretching process. During the recovery process, the cavities created in the matrix due to the stretching were expected to shrink back to their original size, completing a cycle during the cyclic test. However, the higher fraction of CNTs in the CNT2.5 composite (in blue) introduced a higher steric resistance, which hindered the recoverability of the created cavities. This means that the matrix not only undergoes the expected recovery process, but also an extra recovery process due to the presence of rigid CNT particles. As a result, the recovery process of the CNT2.5 composite contained an extra step, leading to a delayed phenomenon in the RCR diagram compared to the composites with a lower fraction of CNTs particles. The sample CNT2.0, on the other hand, exhibited the best sensing behavior due to its optimal CNT content that allowed for efficient stretch and recovery of the matrix without causing excessive steric hindrance.

3.5. Electromagnetic Wave Absorption Performance

In contrast, the imaginary part (ε") of the complex dielectric constant of the CNT2.0 membrane, as shown in Figure 10a, exhibits an increasing trend with the increasing frequency, indicating that polarization relaxation loss dominates over conduction loss in the material. This is supported by the fact that the imaginary part of the complex permeability (μ") also increases with frequency in Figure 10b, indicating the presence of magnetic loss in the material. The magnetic loss is caused by the eddy current generated by the alternating electromagnetic field, which dissipates energy as heat. The overall trend of the real part of the complex permeability (μ') in Figure 10b is relatively stable with a slight decrease at higher frequencies, which indicates that the magnetic properties of the CNT2.0 membrane are less affected by frequency. The combination of these electromagnetic properties suggests that the CNT2.0 membrane has potential as a microwave absorbing material, particularly in the high-frequency range. Magnetic loss also contributes to the dissipation of electromagnetic energies. The general magnetic loss mechanism includes natural resonance, exchange resonance, and vortex loss. As is shown in Figures 5b, μ' and μ" reveal no obvious dependence on frequency. μ" appears to be stable at low-frequency. The small formants of μ' appeared due to natural resonance. Also, more obvious formants appear at high-frequency which are caused by exchange resonance.

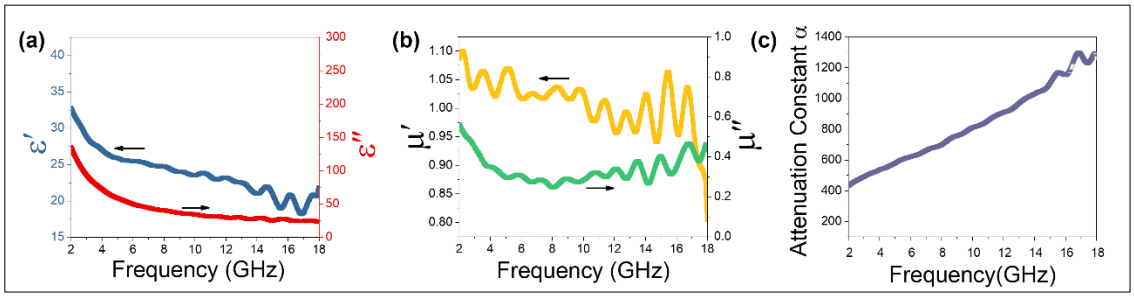

Figure 10. Electromagnetic parameters for the membrane, (a) Real dielectric constant ε' and imaginary dielectric constant ε", (b) real permeability μ' and imaginary permeability μ", (c) attenuation constant α

Moreover, the attenuation constant, which refers to the attenuation or loss of electromagnetic waves upon entering the absorbing material, can be calculated using an equation [28-30]:

$$\alpha = \frac{\sqrt{2}\pi f}{c} \times \sqrt{(\mu''\varepsilon'' - \mu'\varepsilon') + \sqrt{(\mu'\varepsilon'' + \mu''\varepsilon')^2 + (\mu''\varepsilon'' - \mu'\varepsilon')^2}} \quad (3)$$

The absorption performance of the composite membrane was further analyzed using the reflection loss (RL) method, which is a common parameter to evaluate the microwave absorption properties of materials [31]. RL represents the amount of energy reflected from the surface of the material, and a

lower value of RL indicates a stronger absorption ability. The RL values of the CNT2.0 composite membrane at different thicknesses and frequencies are shown in Fig. 11. It can be observed that the RL values of the CNT2.0 composite membrane are all below −10 dB, which indicates excellent microwave absorption properties. Moreover, the RL value decreases with the increasing thickness of the composite membrane at a certain frequency. This is because thicker composites can provide a longer absorbing path, leading to more chances for electromagnetic wave absorption. In addition, at a certain thickness, the RL value decreases with increasing frequency, indicating that the absorption performance of the CNT2.0 composite membrane is more efficient at higher frequencies. This is due to the fact that higher frequency electromagnetic waves have shorter wavelengths, which can interact more easily with the CNTs in the composite and produce more absorption. Overall, the complex dielectric and permeability properties, as well as the RL analysis, suggest that the CNT2.0 composite membrane has promising potential as an effective microwave absorbing material.

The electromagnetic absorption performance of the composite membrane can be evaluated using the transmission line theory and the following equations [32-35]:

$$Z = |Z_{in}/Z_0| = \sqrt{|\mu_r/\varepsilon_r|}\, tanh\left[j\left(\frac{2\pi f d}{c}\right)\right]\sqrt{\mu_r \varepsilon_r} \quad (4)$$

$$RL = 20\, log|(Z_{in} - Z_0)/(Z_{in} + Z_0)| \quad (5)$$

where Z_{in} is the input impedance of the aerogel, f is the frequency, c is the speed of light, d is the thickness of the aerogel, and Z_0 is the impedance in free space. The effectiveness of electromagnetic wave (EMW) absorption is commonly evaluated by the reflection loss (RL) value, which represents the attenuation or loss of EMW radiation after it enters the absorbing material. A RL value of -50 dB indicates that 90% of the incident EMW radiation is absorbed, and the corresponding bandwidth provides information about the effective absorption bandwidth (EAB) [36,37]. In the case of the SEBS/CNTs membrane, as shown in Figure 11a, the RL_{min} value is -4 dB at 16.8 GHz for a thickness of 1.0 mm. The optimization of impedance matching ($|Z_{in}/Z_0|$) results in excellent EMW absorption performance. A value of 1 for $|Z_{in}/Z_0|$ indicates that the absorber has a great impedance match, allowing EMW to easily enter the interior of the membrane. Figure 11d shows that the value of $|Z_{in}/Z_0|$ reaches its maximum value for the membrane with a thickness of 1.0 mm, indicating that the incident EMW can effectively enter the interior of the membrane and be converted into heat to be consumed to avoid reflection at the interface with air.

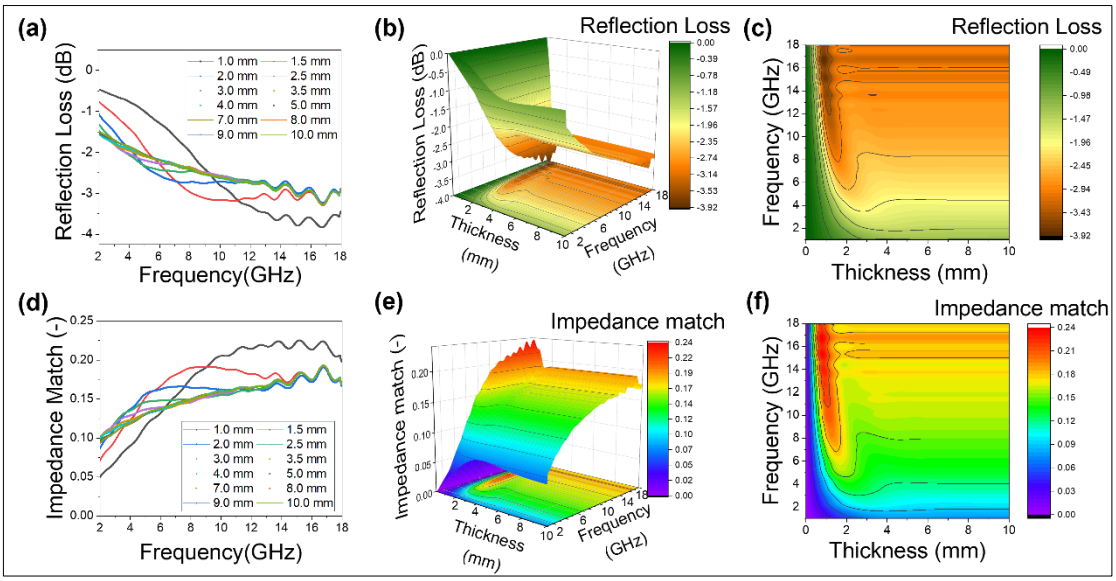

Figure 11. Electromagnetic wave absorption performance of the SEBS/CNTs composite membrane. (a) RL values as a function of frequency and thickness, (b) 3D representation of RL values, and (c) 2D representation of RL values. (d) Z values as a function of frequency and thickness, (e) 3D representation of Z values, and (f) 2D representation of Z values

In addition, Figure 11b and c depict 3D plots and 2D RL diagrams for the SEBS/CNTs composite membrane at various thicknesses within the 2-18 GHz frequency range. Corresponding 3D and 2D diagrams for the impedance (Z) of the SEBS/CNTs composite membrane with respect to thickness and frequency are presented in Figure 11e and f, respectively. The impedance values of the SEBS/CNTs composite membrane with a thickness of 1-2 mm typically fall within the range of 0.12-0.23 at frequencies from 8 to 18 GHz, indicating excellent impedance matching as a contributing factor to its outstanding EMW-absorbing properties.

4. Conclusions

This study focused on the production and characterization of SEBS/CNTs composite membranes with different CNTs fractions. Morphological analysis and TGA measurements were used to determine the structure and content of the CNTs in the composites. The composite with 2.0 wt. % CNTs was found to have the highest elongation at break, acceptable tensile strength, and Young's modulus. The percolation threshold of the SEBS/CNTs composites membrane was determined to be 1.73% using the Mclachlan equation. The cyclic strain sensing behavior of the composite membranes was investigated, and a sketch based on the steric resistance of the CNTs particles was proposed to explain the delayed signal phenomena observed in samples with higher CNTs contents. Finally, the SEBS/CNTs composite membrane with 2 wt.% of CNTs showed superior electromagnetic wave absorption performance, with a minimum reflection loss (RLmin) value. Overall, this study provides fundamental insights into the electrical and mechanical behavior, as well as the EMW absorption of the SEBS/CNTs composite membrane. The findings could guide the development of sensor applications based on mass industrial production of the composite membranes.

Acknowledgement： This work was supported by the Science and Technology Bureau of Jiaxing City [Grant Number 2022AY10006].

Reference

1. LUNA, C. B. B., SIQUEIRA, D. D., ARAÚJO, E. M., NASCIMENTO, E. P., COSTA AGRA DE MELO, J. B., Evaluation of the SEBS copolymer in the compatibility of PP / ABS blends through mechanical, thermal, thermomechanical properties, and morphology. Polymers for Advanced Technologies, 2021, 33 (1), 111-124.
2. WU, T., HU, Y., RONG, H., WANG, C., SEBS-based composite phase change material with thermal shape memory for thermal management applications. Energy, 2021, 221.
3. PANAITESCU, D. M., VULUGA, Z., SANPOREAN, C. G., NICOLAE, C. A., GABOR, A. R., TRUSCA, R., High flow polypropylene/SEBS composites reinforced with differently treated hemp fibers for injection molded parts. Composites Part B: Engineering, 2019, 174.
4. LUNA, C. B. B., SIQUEIRA, D. D., ARAÚJO, E. M., WELLEN, R. M. R., Tailoring PS/PPrecycled blends compatibilized with SEBS. Evaluation of rheological, mechanical, thermomechanical and morphological characters. Materials Research Express, 2019, 6 (7).
5. ZHANG, Z. X., DAI, X. R., ZOU, L., WEN, S. B., SINHA, T. K., LI, H., A developed, eco-friendly, and flexible thermoplastic elastomeric foam from SEBS for footwear application. Express Polymer Letters, 2019, 13 (11), 948-958.
6. AL MUNSUR, A. Z., HOSSAIN, I., NAM, S. Y., CHAE, J. E., KIM, T.-H., Hydrophobic-hydrophilic comb-type quaternary ammonium-functionalized SEBS copolymers for high performance anion exchange membranes. Journal of Membrane Science, 2020, 599.
7. BANERJEE, S. S., BURBINE, S., KODIHALLI SHIVAPRAKASH, N., MEAD, J., 3D-Printable PP/SEBS Thermoplastic Elastomeric Blends: Preparation and Properties. Polymers (Basel), 2019, 11 (2).

8. LI, T.-T., DAI, W., HUANG, S.-Y., WANG, H., LIN, Q., LOU, C.-W., LIN, J.-H., Preparation and characterization of SEBS-g-MAH-filled flexible polyurethane foam composites with gradient-changing structure. Materials & Design, 2019, 183.
9. HE, Y., WU, D., ZHOU, M., ZHENG, Y., WANG, T., LU, C., ... LIU, C., (2021), Wearable strain sensors based on a porous polydimethylsiloxane hybrid with carbon nanotubes and graphene. ACS Applied Materials & Interfaces, 13(13), 15572-15583.
10. LEE, J., PYO, S., KWON, D. S., JO, E., KIM, W., KIM, J., (2019), Ultrasensitive strain sensors based on separation of overlapped carbon nanotubes. *Small*, *15*(12), 1805120.
11. QU, M., FANG, J., MU, C., LI, Y., HUANG, S., HAN, L., ... QIN, Y., (2022), A novel study on the sandwich-structure strain sensor using ethylene-vinyl acetate-based hot-melt adhesive mesh web: Fabrication, properties, and modeling. *Journal of Applied Polymer Science*, *139*(48), e53209.
12. CUI, X., JIANG, Y., XU, Z., XI, M., JIANG, Y., SONG, P., ZHAO, Y., WANG, H., Stretchable strain sensors with dentate groove structure for enhanced sensing recoverability. Composites Part B: Engineering, 2021, 211.
13. PADOVANO, E., BONELLI, M. E., VECA, A., DE MEO, E., BADINI, C., Effect of long-term mechanical cycling and laser surface treatment on piezoresistive properties of SEBS-CNTs composites. Reactive and Functional Polymers, 2020, 152.
14. PAN, S., PEI, Z., JING, Z., SONG, J., ZHANG, W., ZHANG, Q., SANG, S., A highly stretchable strain sensor based on CNT/graphene/fullerene-SEBS. RSC Adv, 2020, 10 (19), 11225-11232.
15. TEKAY, E., Preparation and characterization of electro-active shape memory PCL/SEBS-g-MA/MWCNT nanocomposites. Polymer, 2020, 209.
16. ZENG, J., MA, W., WANG, Q., YU, S., INNOCENT, M. T.; XIANG, H.; ZHU, M., Strong, high stretchable and ultrasensitive SEBS/CNTs hybrid fiber for high-performance strain sensor. Composites Communications 2021, 25.
17. XU, Y., TANG, S., PAN, J., BAO, J., ZHANG, A. J. M., Design, Reversibly cross-linked SEBS/carbon hybrid composite with excellent solvent-proof and electromagnetic shielding properties, 2018, 146, 1-11.
18.KIM, H., PARK, S., KIM, S., SEO, Y. J. L., Microwave absorption and shielding property of Fe–Si–Al alloy/MWCNT/polymer nanocomposites, 2019, 35 (21), 6950-6955.
19.HUANG, H., WANG, W., HUA, M., KUANG, J., MA, Y., GUO, Z.; XIE, W. J. P. B. C. M., Broadband radar absorbing characteristic based on periodic hollow truncated cone structure, 2020, 595, 412368.
20.WU, L., WANG, L., GUO, Z., LUO, J., XUE, H., GAO, J. J. A. a. m.; interfaces, Durable and multifunctional superhydrophobic coatings with excellent joule heating and electromagnetic interference shielding performance for flexible sensing electronics, 2019, 11 (37), 34338-34347.
21.HUANG, H., WANG, W., CAO, T., KUANG, J., DENG, Y., HUA, M., XIE, W. J. C. S., Broadband radar absorbing performance of corrugated structure, 2020, 253, 112809.
22. STAUFFER D., AHARONY A., REDNER S., Introduction to Percolation Theory[J]. Physics Today, 1987, 40(4):64-64.
23. LUO, X., QU, M., SCHUBERT, D. W., (2021), Electrical conductivity and fiber orientation of poly (methyl methacrylate)/carbon fiber composite sheets with various thickness. *Polymer Composites*, *42*(2), 548-558.
24.QU, M., LI, D., QIN, T., LUO, Z., LIU, X., NILSSON, F., ... QIN, Y., (2022), Carbon Black Nanoparticle/Polydopamine-Coated Core-Spun Yarns for Flexible Strain Sensors. *ACS Applied Nano Materials*, *5*(11), 16996-17003.
25. QU, M., QIN, Y., XU, W., ZHENG, Z., XU, H., SCHUBERT, D. W., GAO, Q., (2021). Electrically conductive NBR/CB flexible composite film for ultrastretchable strain sensors: Fabrication and modeling. *Applied Nanoscience*, *11*, 429-439.

26. DUAN, L., FU, S., DENG, H., ZHANG, Q., WANG, K., CHEN, F., FU, Q., (2014), The resistivity–strain behavior of conductive polymer composites: stability and sensitivity. *Journal of Materials Chemistry A*, *2*(40), 17085-17098.
27. NATARAJAN, T. S., ESHWARAN, S. B., STÖCKELHUBER, K. W., WIEßNER, S., PÖTSCHKE, P., HEINRICH, G., Das, A., (2017), Strong strain sensing performance of natural rubber nano-composites. ACS applied materials & interfaces, 9(5), 4860-4872.
28. CHENG, Y., LI, Z., LI, Y., DAI, S., JI, G., ZHAO, H., ... DU, Y., (2018), Rationally regulating complex dielectric parameters of mesoporous carbon hollow spheres to carry out efficient microwave absorption. *Carbon*, *127*, 643-652.
29. CHEN, H., HUANG, Z., HUANG, Y., ZHANG, Y., GE, Z., QIN, B., ... CHEN, Y., (2017), Synergistically assembled MWCNT/graphene foam with highly efficient microwave absorption in both C and X bands. *Carbon*, *124*, 506-514.
30. SONG, L., ZHANG, F., CHEN, Y., GUAN, L., ZHU, Y., CHEN, M., ... FAN, B., (2022), Multifunctional SiC@ SiO_2 nanofiber aerogel with ultrabroadband electromagnetic wave absorption. *Nano-Micro Letters*, *14*(1), 152.
31. WANG, X., QIN, J., CUI, J., HUANG, L., YUAN, Y., LI, Y., (2022), Reduced graphene oxide/carbon nanofiber based composite fabrics with spider web-like structure for microwave absorbing applications. *Advanced Fiber Materials*, *4*(5), 1164-1176.
32. WU, F., LIU, Z., XIU, T., ZHU, B., KHAN, I., LIU, P., ... ZHANG, B., (2021), Fabrication of ultralight helical porous carbon fibers with CNTs-confined Ni nanoparticles for enhanced microwave absorption. *Composites Part B: Engineering*, *215*, 108814.
33. CHE, R. C., ZHI, C. Y., LIANG, C. Y., ZHOU, X. G., (2006), Fabrication and microwave absorption of carbon nanotubes⁄ $CoFe_2O_4$ spinel nanocomposite. *Applied Physics Letters*, *88*(3), 033105.
34. SUN, H., CHE, R., YOU, X., JIANG, Y., YANG, Z., DENG, J., ... Peng, H., (2014), Cross-stacking aligned carbon-nanotube films to tune microwave absorption frequencies and increase absorption intensities. *Advanced materials*, *26*(48), 8120-8125.
35. LIU, J., CHE, R., CHEN, H., ZHANG, F., XIA, F., WU, Q., WANG, M., (2012), Microwave absorption enhancement of multifunctional composite microspheres with spinel Fe_3O_4 cores and anatase TiO2 shells. *Small*, *8*(8), 1214-1221.
36. HUANG, B., WANG, Z., HU, H., HUANG, X., YUE, J., WANG, Y., (2020), Enhancement of the microwave absorption properties of PyC-SiCf/SiC composites by electrophoretic deposition of SiC nanowires on SiC fibers. *Ceramics International*, *46*(7), 9303-9310.
37.ZHANG, K. L., ZHANG, J. Y., HOU, Z. L., BI, S., ZHAO, Q. L., (2019), Multifunctional broadband microwave absorption of flexible graphene composites. *Carbon*, *141*, 608-617.

Manuscript received: 13.05.2023